SEGMENTATION AND DENSITY-EVALUATION OF FIBER-REINFORCED MATERIALS BY DUAL-ENERGY COMPUTERIZED TOMOGRAPHY

U. Hassler, P. Rizo
LETI (CEA - Technologies Avancées), Département Systèmes
17, rue des Martyrs, 38054 Grenoble, France

L. Garnero
Institut d'Optique
Université de Paris-Sud, France

INTRODUCTION

This work has been prepared within the Brite-Euram project "DUALETO", whose purpose is the development of a high-resolution Dual-Energy computerized tomography system (DE-CT). It is dedicated to non-destructive inspection of fiber-reinforced ceramic parts. The DE-measurement will be acquired simultaneously by an energy- and position-sensitive line detector. Using an appropriate calibration function, these DE-acquisitions are used to calculate the distributions of mass density of the ceramic's two components and with them, the volumic fraction (VF) of fibers in the matrix material. Due to several reasons, these density data are very noisy. This paper presents a method for obtaining mass density data with a lower level of noise. For this, structural information about object, defects and bundles of fibers are derived from the low-energy measurement and stored in label images. Structure information is then used to perform a non-linear filtering on mass density data, in order to estimate the volumic fraction.

The first section of the paper briefly recalls the principle of the Dual-Energy method. Then, the parameters of the generation of simulated DE-data for a slice of a SiC/C sample are presented. Thereafter, the transformation of DE-data into mass density data by means of an a priori calibration procedure is described. The following section about segmentation details the creation of label images for storage of structural information. In the final section, the filtering of mass density data is presented, and the results of the proposed method obtained on simulated data are compared with another segmentation method based on Markov random fields.

DUAL-ENERGY COMPUTED TOMOGRAPHY

A well established method for visualizing internal structures of an object is X-ray CT. A set of measurements of X-ray intensity transmitted through an object is acquired. Under the assumption that the X-ray energy spectrum can be approximated by an average energy, the set of projections is transformed by a reconstruction process into an image of attenuation coefficients. These coefficients however are not of quantitative nature, since the

Review of Progress in Quantitative Nondestructive Evaluation, Vol. 15
Edited by D.O. Thompson and D.E. Chimenti, Plenum Press, New York, 1996

usually used radiation is polychromatic and the attenuation of radiation is an energy-dependent and non-linear process. For a given material (atomic number $Z < 20$) and energies below 200 keV, the attenuation process can be well approximated by two parameters, which represent the physical processes of absorption and diffusion of photons by electrons [1]. Two measurements using sufficiently differing bands of energy allow the determination of these two parameters and thereby the restauration of energy-dependent information [2]. If the investigated object consists of two materials, then quantitative images of the density distribution of the two materials can be reconstructed separately [3]. However, to get a quantitative measure of chemical composition and/or mass density, calibration functions have to be found, which provide the relationship between a pair of intensity-measurements *mes* of the detector into a pair of mass projections M of two basis materials:

$$f_{cal} : \begin{pmatrix} mes_{low} \\ mes_{high} \end{pmatrix} \longrightarrow \begin{pmatrix} M_{mat1} \\ M_{mat2} \end{pmatrix}, \tag{1}$$

where

$$M_{mat_i} = \int_{ray} \rho_{mat_i} \tag{2}$$

is the surfacic mass $[\frac{g}{cm^2}]$ of material i along the projection ray. Projections in terms of the surfacic mass will be transformed into an image of mass density values by the reconstruction process. As a consequence of the energy-dependent attenuation of matter, of the usually polychromatic and overlapping spectra of the two measurements as well as of non-linearities of the detector, the calibration functions have a non-linear behavior. One possibility to find f_{cal} for a given system is to pretend a general form like polynomials of 2. or 3. degree. The unknown coefficients can then be determined by measuring reference objects of perfectly known composition followed by an inversion procedure [2-4].

One of the problems of the DE-method is the amplification of noise. Two measurements independently corrupted by photonic noise are combined by only imperfectly known calibration functions. This level of noise is further amplified by the final reconstruction process. For getting an idea of the amplitude of noise, a simulation of the DE-processing chain was made. A filtered backprojection algorithm (FBP) is used for the reconstruction process.

GENERATION OF SIMULATED DE-DATA

As energy spectrum of X-radiation, tabulated values for a 17° tungsten target at 140 keV and with a 2.5 mm Al-filter from Birch et al. [5] are used (Fig. 1a). The number of emitted photons I(E) of each energy (1 keV step) follows a poisson process N_P. The detector has 512 cells of 0.21x0.30 mm^2 (width x heigth). Its sensitivity D(E) in the low energy band goes from 75% at 28 keV to 90% at 42 keV, whereas in the high energy domain, it goes from 75% at 80 keV down to 40% at 120 keV (Fig. 1b). These values are taken from Besch et al. [6]. Furthermore, the detector signal is additionally corrupted by gaussian noise N_G with a variance of 10% of the signal. The object is positionned so that a pixel size of 30 x 30 μm^2 is reached in the reconstructed image.

The slice of the simulated object has a diameter of 14 mm and contains fibers oriented perpendicularly to the line-detector. The fibers are modelized by circles having a diameter between $10\mu m$ and $20\mu m$ and are grouped by bundles. The volumic fraction (VF) of fibers is between 30% to 45% in bundles, whereas the matrix contains sparsely distributed fibers with an average VF of 10%. The material of the matrix is SiC with a density of $2.3\frac{g}{cm^3}$, and the fibers are of C with a density of $1.8\frac{g}{cm^3}$. Mass attenuation coefficients c(E) of the materials are taken from Storm and Israel [7] and are shown in figure 1c. The slice contains 12 holes sized from 50 x 100 μm^2 to 100 x 500 μm^2.

For each projection angle (750 steps in 360°) and for each detector cell (512), the

length of a X-ray passed through each of the two materials, is calculated. With these two lengths l_{mat1} and l_{mat2}, values mes_{low} and mes_{high} of a hypothetical DE-measurement can be computed according to the following formula:

$$mes = \int_{E_1}^{E_2} I(E)\, N_P\, D(E)\, N_G\, e^{-(c_{mat1}(E)\rho_{mat1}l_{mat1}+c_{mat2}(E)\rho_{mat2}l_{mat2})} dE. \quad (3)$$

An acquisition time of 5 seconds is assumed. Scattered photons are neglected, assuming a long distance between object and detector and the collimation function of the entrance window of the detector [6].

A PRIORI CALIBRATION

In contrast to conventional calibration, where samples of exactly known composition are necessary, the a priori calibration uses existing a priori information about spectrum, materials and detector in order to replace real calibration measurements. The result of the a priori calibration procedure consists in calibration functions, whose coefficients are determined by simulating the measurements of reference objects under the assumption of a priori known system parameters. For inversion, a singular value decomposition method, described by Rizo and Robert in [3], is used. For the above mentioned system parameters, we obtain the following functions for transforming two intensity measurements mes_{low} and mes_{high} into two mass projections M_{mat1} and M_{mat2}:

$$M_{mat1} = 2.07mes_{low} - 3.06mes_{high} - 0.41mes_{low}mes_{high} + 0.18mes_{low}^2 + 0.23mes_{high}^2 \quad (4)$$

$$M_{mat2} = -2.47mes_{low} + 10.14mes_{high} + 0.48mes_{low}mes_{high} - 0.21mes_{low}^2 - 0.28mes_{high}^2 \quad (5)$$

Mass projections of the two materials are now transformed by the FBP reconstruction process into mass density images of SiC and C, respectively. A section of the simulated slice, a histogram of density values and a profile through the slice is shown in Figure 2 for each of the two materials. As a consequence of noise propagation, it is very difficult to recognize the structure of the object (bundles of fibers). Moreover, one can find in both images theoretically impossible negative values of densities and values above the maximum density. As one can clearly see, the C-image is much noisier than the SiC-image. The different levels of noise can be explained by the fact that the fibers image depends more on the high-energy measurement (Eq. 5), where the number of emitted photons and the counting efficiency of the detector are lower and the attenuation coefficients of the two materials are less different (Fig. 1a-c). Therefore, a further processing stage is required in order to reduce the noise level.

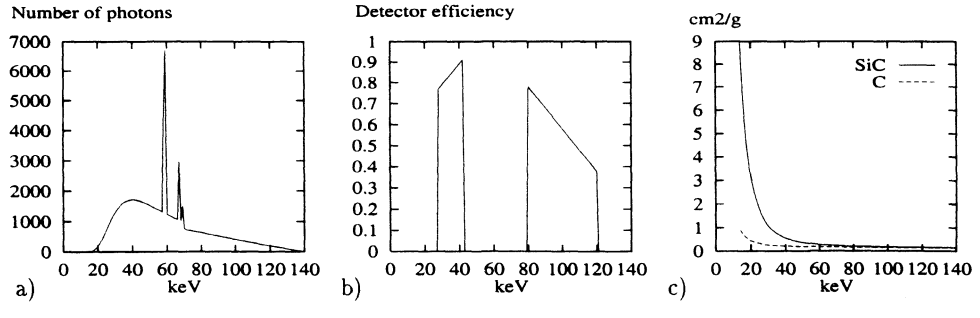

Figure 1: a) Energy spectrum [number of photons], b) detector efficiency and c) mass attenuation coefficients of materials $[cm^2/g]$

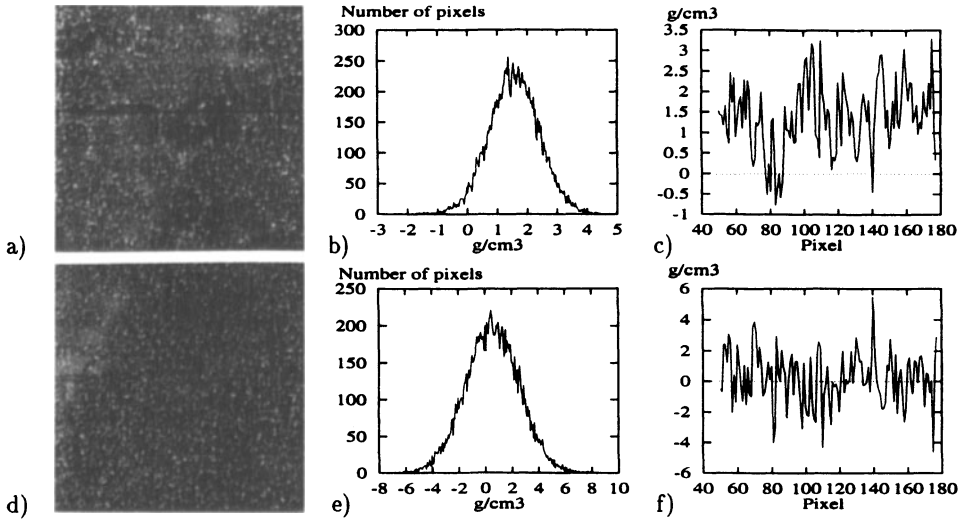

Figure 2: a) Section of reconstructed SiC- density image, b) histogram of density values of SiC, c) profile through slice, d) - f) analogically for C-material

SEGMENTATION

General Proceeding

In order to reduce the noise level in density data, low-pass filtering of the image data can be used, that is to say, the density of a point is computed by taking the average density in a certain neighbourhood of this point. However, this averaging smears edges between neighbouring structures and can destroy important information especially about little objects like holes. Therefore, a selective filtering is more appropriate, which averages only pixels belonging to the same class of objects. For doing this, a classification of the image pixels into one of the possible object classes is necessary. This classification can be seen as the recovering of only the structural information of the object, and the pixel content can be expressed by a symbolic and non-quantitative label. An advantage of such a qualitative processing is, that directly a reconstruction of the low-energy measurement (Fig. 3) can be used, which has a much lower level of noise (no calibration) and a higher contrast than the mass projections.

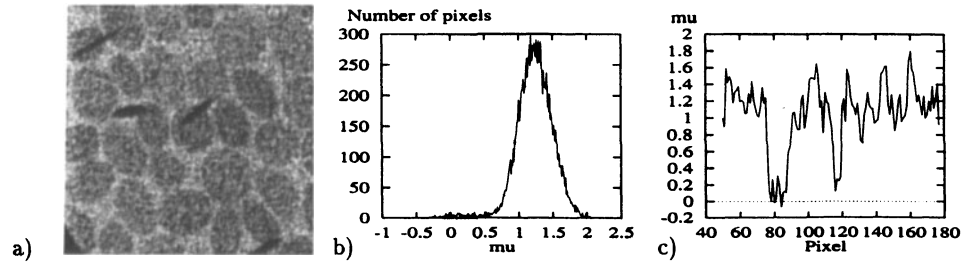

Figure 3: a) Section of reconstructed low-energy measurement, b) histogram of the linear attenuation coefficient μ and c) profile through slice

Label Classes

For the inspection of composites, 4 classes of image contents have to be distingished: *background*, *matrix*, *bundles* of fibers and *holes*. Since the fiber size is smaller than pixel size, an exact location of all fibers in the matrix is not possible, so a segmentation into regions with high and low portion of fibers has to be done. If one introduces the two additional labels *object* and *material*, the total set of labels can be expressed by a label tree (Fig. 4), and the classification can be done in 3 steps, where at each step one label image is created and only two different classes have to be separated. Each label image has a predefined depth of n bits ($n \geq 2$), which allows to express several degrees of uncertainty. In the presented example, the depth of the OBJECT-, MATERIAL- and BUNDLE-images is 2, 3 and 4 bits respectively.

Segmentation of Image Data

The creation of a label image consists in an initialization-step followed by iterated median filtering for noise reduction and region growing. Initialization of a label image L is done by a step function, which transforms data of image R into the label domain $[0, 2^n - 1]$:

$$L(x,y) = \begin{cases} 0 & \text{if } R(x,y) < h_{min} \\ 2^n - 1 & \text{if } R(x,y) > h_{max} \\ \left\lfloor 2^{n-1} \frac{R(x,y) - h_{min}}{h_{max} - h_{min}} \right\rfloor + 1 & \text{otherwise} \end{cases}, \tag{6}$$

where h_{min} and h_{max} are two threshold values. For the discrimination of two classes, it is assumed that pixels with values below h_{min} belong to the opposite class than pixels above h_{max}. Pixels between h_{min} and h_{max} are quantized into 2^{n-1} different values. Such intermediate label values can either be interpreted as uncertain classification (L_1) or as different levels of VF (L_3).

For reducing acquisition and reconstruction noise, the initialized label image is filtered by a median filter, which is defined as:

$$\text{Median}(x_i) = x'_{(N+1)/2}, \tag{7}$$

where x_i is a series of N integers of a window of size m × m (m odd) and x'_i is a sorted series with $x'_n \leq x'_{n+1}, n = 0, \ldots, N-1$. The median filter has some interesting properties:

- suppression of impulsive noise while preserving edges [8]
- non-parametric estimator for the center of a distribution [9]
- converging behavior for iterated application [10]
- fast algorithms [11]

Therefore the median seems to be an appropriate method to reduce noise level in the label images. On simulated data, a good convergence was reached after two iterations.

The evolution of the label images is shown in Figure 5.
In the first step for separation of object and background, h_{min} is set to 0 under the assumption, that a pixel with an attenuation coefficient of 0 represents no matter. h_{max} is chosen to be 0.4 representing any kind of matter. All pixels inside the outermost object-labels are treated as belonging to the object (including holes in the object). A window size of 5 × 5 pixels is used for median filtering. The second step consists in the

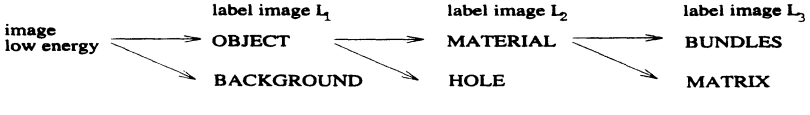

Figure 4: Hierarchical label tree for successive classification of image contents into background, pores, matrix and bundles of fibers.

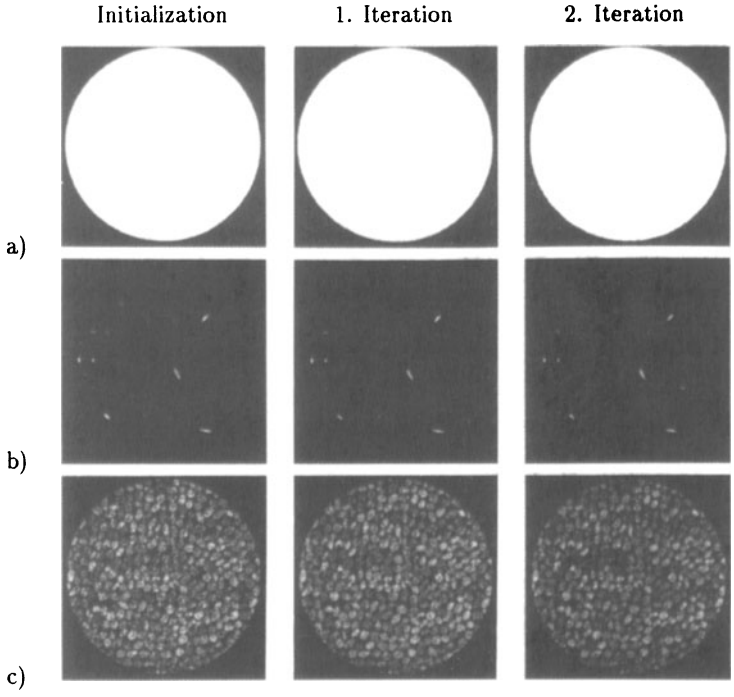

Figure 5: a) Label image L_1, separation of object from background, b) L_2, separation of material from holes, c) L_3, separation of bundles of fibers from matrix

location of the holes in the object. Only pixels having the label *object* are considered. Again, h_{min} is set to 0. The value for h_{max} is estimated to be 1, representing the attenuation coefficient of a pixel containing only the material with lowest attenuation. The window size for the median is 3×3. All the simulated holes can be located.

The last step is to classify the pixels with *material*-label into matrix and bundles of fibers. In this case, no predefined values for h_{min} and h_{max} can be used, therefore they are derived from the histogram h of the pixels with label *material.* It is supposed, that h is a superposition of the two material distributions, then h_{min} and h_{max} are determined using the following relations:

$$P(x \leq h_{min}) = 0.05 \quad \text{and} \quad P(x \geq h_{max}) = 0.05, \quad x \in h. \tag{8}$$

Median filtering is done again with a 3×3 mask. An advantage of such a processing is, that no material-dependent parameter is needed for separation of matrix and bundles of fibers.

FILTERING OF DENSITY DATA

The label images produced by the segmentation process are now used to do a selective filtering of the previously computed mass density images. Figure 6 shows the entire data-flow for computing filtered density images. Function f_{filt} accomplishes the following task: For every pixel having a *material* label l, an average density within a mask is computed, using all the pixels having the same label l.

Results

The best results are obtained for a mask radius of 7 pixels. The resulting filtered density images are shown Figure 8. A comparison with theoretically correct density data indicates, that the mean error per pixel was reduced from 0.67 $\frac{g}{cm^3}$ (unfiltered) to 0.20 $\frac{g}{cm^3}$ for density of SiC and from 1.78 $\frac{g}{cm^3}$ (unfiltered) to 0.27 $\frac{g}{cm^3}$ for density of C.

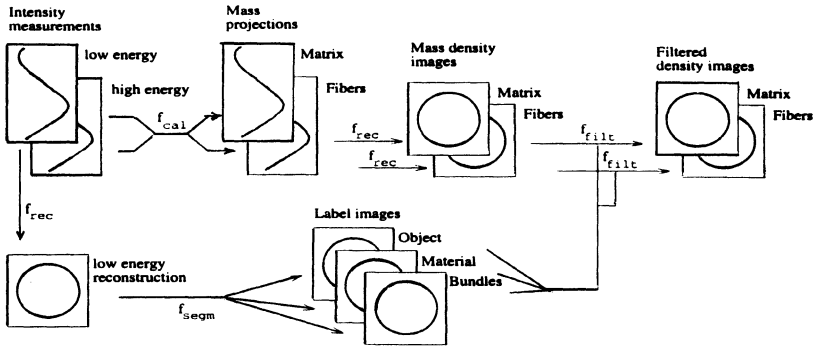

Figure 6: Data flow for computing filtered density images of the matrix and fibers material using label images.

Comparison with a Bayesian Segmentation Method

Within the Brite project, another segmentation method has been developed for enhancing image quality of DE-measurements by C. Robert et al., [12]. That method also uses label images for filtering density images, but the label images are computed by maximizing the a posteriori probability of the solution according to the rule of Bayes. A priori information, such as geometrical constraints can be introduced by a Markov random field. This method needs class specific parameters, which have to be estimated from density images in a separate training phase. Table 1 shows an opposition of the results of the two methods and the theoretical correct values. The test consisted in evaluating the average material content in 6 regions of the simulated object presented above. It can be stated that the performance is about equal for determination of matrix content, whereas the Bayesian method works better in the case of determination of fibers content.

CONCLUSION

The presented paper described a method for deriving mass density information from Dual-Energy measurements. Two intensity measurements are transformed into mass projections by means of a calibration procedure using existing a priori information about the system. The high level of noise in density data is reduced by a non-linear filter using structural information about the object. The structural information is created by a segmentation process and stored in label images. For a validation of this approach, a simulation of a DE-acquisition has be done for a SiC/C sample. The mean error of density is reduced considerably by the presented method. Future work will be dedicated to a validation of the proposed method with real acquisitions. Especially the assumption of a priori knowledge for spectrum and detector has to be verified.

ACKNOWLEDGEMENT

This work was sponsored by the European Community project Brite-Euram BRE5535 "DUALETO".

Table 1: Comparison of two segmentation methods.

	Matrix content [%]						Fibers content, VF [%]					
Region	1	2	3	4	5	6	1	2	3	4	5	6
Theoretical value	69	67	69	54	57	56	31	33	31	46	43	44
Bayesian method	68	66	69	56	56	55	32	35	29	41	45	45
Median method	68	67	69	57	56	55	32	32	28	40	46	46

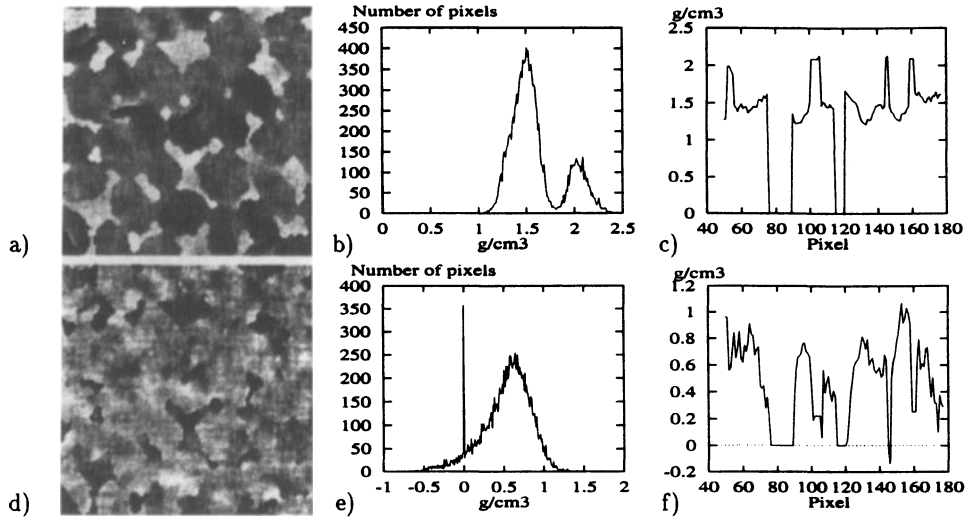

Figure 7: a) Section of filtered SiC- density image, b) histogram of density values, c) profile through slice, d)-f) analogically for C-material.

REFERENCES

1. R.A. Rutherford, B.R. Pullan, I. Isherwood, "Measurement of Effective Atomic Number and Electron Density Using an EMI Scanner", Neuroradiology 11, 16-21 (1976)
2. R.E. Alvarez, A. Macovski, "Energy-selective Reconstructions in X-ray Computerized Tomography", Phys. Med. Biol. 21, No. 5, pp. 733-744 (1976)
3. P. Rizo, C. Robert, "Dual-Energy Tomography for Ceramics and Composites Materials", *Proc. of International Symposium on Computerized Tomography for Industrial Applications*, Berlin, June 8-10, 1994, pp. 128-135
4. J. Coumans, "Doppel-Energie Computer-Tomographie und -Radiographie", Dissertation, University of Braunschweig, Germany, 1984
5. Birch, Marshall, Ardran, *Cataloque of spectral data for diagnostic X-rays*, The Hospital Physicists Association, Scientific report Series 30
6. H.J. Besch, T. Feige et al., "A position sensitive and energy-selective single photon counter for X-ray precision tomography", *Proc. of International Symposium on Computerized Tomography for Industrial Applications*, Berlin, June 8-10, 1994, pp. 369-376
7. E. Storm, H. Israel, *Photon cross sections from 1 keV to 100 MeV for elements Z=1 to Z=100*, Academic Press Inc., 1970
8. H. Niemann, *Pattern Analysis and Understanding*, Springer, Berlin, 1990
9. C.G. Small, "A Survey of Multidimensional Medians", International Statistical Review 58, No. 3, pp. 263-277 (1990)
10. J.P. Fitch, E.J. Coyle, N.C. Gallagher, "Root Properties and Convergence Rates of Median Filters", IEEE ASSP 33, No. 1, pp. 230-240, (1985)
11. T.S. Huang, G. Yang, G. Tang, "A fast two dimensional median filtering algorithm", IEEE ASSP 27, pp. 13-18, (Feb. 1979)
12. C. Robert, J.-M. Dinten, P. Rizo, "Dual-energy computed tomography (CT) for ceramics and composites materials", to be presented in 22. Annual Review of Progress in QNDE, Jul. 31 - Aug. 4, 1995, Seattle, USA